Impurity scattering effects on the superconducting properties and the tetragonal-to-orthorhombic phase transition in FeSe

M. Abdel-Hafiez,[1,2,*] Y. J. Pu,[3] J. Brisbois,[4] R. Peng,[3] D. L. Feng,[3] D. A. Chareev,[5,6] A. V. Silhanek,[4] C. Krellner,[2] A. N. Vasiliev,[6,7,8] and Xiao-Jia Chen[1,†]

[1]*Center for High Pressure Science and Technology Advanced Research, Shanghai 201203, China*
[2]*Institute of Physics, Goethe University Frankfurt, 60438 Frankfurt am Main, Germany*
[3]*Department of Physics and Advanced Materials Laboratory, Fudan University, Shanghai 200433, China*
[4]*Département de Physique, Université de Liège, B-4000 Sart Tilman, Belgium*
[5]*Institute of Experimental Mineralogy, Russian Academy of Sciences, 142432 Chernogolovka, Moscow District, Russia*
[6]*Institute of Physics and Technology, Ural Federal University, 620002 Ekaternburg, Russia*
[7]*Low Temperature Physics and Superconductivity Department, Physics Faculty, M.V. Lomonosov Moscow State University, 119991 Moscow, Russia*
[8]*National University of Science and Technology "MISiS," Moscow 119049, Russia*

(Received 8 December 2015; revised manuscript received 9 May 2016; published 8 June 2016)

A comprehensive study of the doping dependence of the phase diagram of FeSe-based superconductors is still required due to the lack of a clean and systematic means of doping control. Here, we report on the magneto-optical imaging, thermodynamic and transport properties, as well as *in situ* angle-resolved photoemission spectroscopy (ARPES) studies of impurity scattering in stoichiometric FeSe single crystals. Co doping at the Fe site is found to decrease the superconducting transition temperature (T_c). The upper critical field and specific heat all indicate a possible multiband superconductivity with strong coupling in the Co-doped system. A remarkable feature in FeSe is that its temperature dependent resistivity exhibits a wide hump at high temperatures, a signature of a crossover from a semiconductinglike behavior to metallic behavior. A structural tetragonal-to-orthorhombic phase transition (T_s) (a consequence of the electronic nematicity) is suppressed by either physical or chemical pressures. Due to the reconstruction of the Fermi surface at T_s, specific heat anomalies at T_s present $\Delta C_p/T_s \approx \gamma_n$, being γ_n the Sommerfield coefficient at low temperature. This reflect an additional electronic instability in the $FeSe_{1-x}S_x$ system. ARPES data between 180 and 282 K indicates the existence of a chemical potential shift with increasing thermal excitations, resulting in a change of the Fermi-surface topology and exhibiting a semimetal behavior. We found that the temperature-induced Lifshitz transition is much higher than the temperature for the nematic order.

DOI: 10.1103/PhysRevB.93.224508

I. INTRODUCTION

The majority of the parent and underdoped compounds of iron-based superconductors exhibit a stripe-type long-range antiferromagnetic order, accompanied by a nematic order [1]. Superconductivity in these materials emerges when the magnetic and nematic order are partially or completely suppressed by chemical doping or by the application of pressure [2,3]. This is because the interaction that drives the nematic order may also mediate the Cooper pairing. This emergence and strengthening of antiferromagnetic order was directly evidenced by muon rotation spectroscopy [4,5]. Therefore, there is a great deal of interest and excitement in understanding the microscopic origin of nematicity in iron-based superconductors. Among iron-based superconductors, FeSe exhibits intriguing and distinctive properties, which are currently the research focus in the field of high temperature superconductors [6–8]. Undoped FeSe possesses a nematic order below 90 K and becomes superconducting below 8 K [9,10]. The most interesting property of these materials is not only the pressure or strain increasing the T_c, but a giant enhancement of the superconductivity at the FeSe/$SrTiO_3$ (STO) interface, where the strain drastically changes the parameters of the magnetic subsystem in FeSe [11]. It seems that STO provides phonons that enhance superconductivity in single-layered FeSe [12,13]. Recently, the superconducting transition was enhanced in K-dosed FeSe. Although the competition between nematicity and superconductivity likely plays an important role in the enhanced superconductivity, it does not imply that this is the single cause behind the observed effect [14].

Whether the nematic order is driven by spin or orbital fluctuations is still hotly debated. The orbital fluctuation mechanism produces a sign preserving s^{++}-wave pairing, where the order parameters of the electron and hole pockets do not change their relative signs [15,16], while the spin fluctuation mechanism favors a sign-changing s-wave pairing, where the electron and the hole Fermi surfaces have order parameters with opposite signs [17,18]. Furthermore, in the spin-fluctuation-based pairing theory the possible existence of order-parameter nodes is reported in both singlet and triplet superconducting states [19,20]. Although impurity scattering shows a pair breaking effect, there are different opinions on the possible pairing symmetry; for instance, the suppression of superconductivity by the Co replacement on the Fe sites [21]. However, superconductivity suppression is much weaker than that expected in a $s^{\pm}$ pairing, and thus supports sign-preserving s-wave pairing. In contrast, in Co-doped $Ba(Fe_{1-x}Co_x)_2As_2$, a believed $s^{\pm}$-pairing superconductor,

*m.mohamed@hpstar.ac.cn
†xjchen@hpstar.ac.cn

increasing the Co concentration leads to an enhancement of the critical temperature T_c up to 26 K, instead of effectively suppressing the superconductivity [22]. Impurity scattering in high temperature superconductors is a critical parameter that governs the electron correlations and ground states. This helps to understand the interplay and mechanism of different phases and investigates rich phase diagrams. Nevertheless, due to the lack of clean and systematic means of a doping control, a comprehensive study of the doping dependence of the phase diagram of an FeSe-based superconductor is still lacking. With the hope of filling this gap, we report here on the effect of impurity scattering on superconductivity and tetragonal-to-orthorhombic phase transition in FeSe. Transport data at higher temperatures in FeSe exhibit a wide hump with a crossover, probably from a semiconductinglike behavior to a metallic behavior. This is supported by angle-resolved photoemission spectroscopy (ARPES) data at higher temperatures, where the data shows a change in the Fermi-surface topology and, therefore, exhibits a semimetal behavior. Additionally, the temperature-induced Lifshitz transition is found to be much higher than the temperature for the nematic order.

II. EXPERIMENT

The conductance anisotropy in layered material single crystals is large, so a traditional four-terminal method measuring the resistivity along the *ab* plane, ρ_{ab}, may be unreliable [23]. In view of this fact, we used six terminals to determine each principal component of resistivity. In the latter method, the current was injected through the outermost contacts on one surface whereas voltages were measured across the innermost contacts of each surface. The Laplace equation was solved and inverted to find ρ_{ab} [24]. In addition, this method allowed the sample homogeneity to be tested by permuting the electrodes which were used for the current and voltage [23,24]. We investigated selected platelike FeSe, $FeSe_{1-x}S_x$, and $Fe_{1-x}Co_xSe$ single crystals, grown in an evacuated quartz ampoule, using the $AlCl_3$/KCl flux technique with a constant temperature gradient of 5 °C/cm along the ampoule length. The temperature of the hot end was kept at 427 °C, and the temperature of the cold end was about 350 − 330 °C. The phase purity of the resulting crystal was checked with x-ray diffraction. The chemical compositions of the crystals were studied using a digital scanning electronic microscope, TESCAN Vega II XMU, with the energy dispersive microanalysis system INCA Energy 450/XT (20 kV). The good quality of the crystals was confirmed by specific-heat jump, a complete superconducting volume, and sharp superconducting transition [25–28]. The resistivity and thermodynamic measurements were measured in a Quantum Design Physical Property Measurement System with an adiabatic thermal relaxation technique. The visualization of the magnetic flux landscape was performed through the Faraday rotation of linearly polarized light in a Bi-doped yttrium iron garnet with in-plane magnetic domains, a technique known as magneto-optical imaging (MOI) [29,30]. This technique requires planar surfaces in order to ensure good proximity of the magneto-optical layer to the sample. To that end, we cleaved large single crystals using a traditional scotch tape method on both sides and thus obtained flat samples on the millimeter scale length. Our ARPES data was gathered under an ultrahigh vacuum of 1.5×10^{-11} mbar, with a SPECS UVLS discharge lamp (21.2 eV He-Iα) and a Scienta R4000 electron analyzer. The energy resolution is 8 meV and the angular resolution is 0.3.

III. RESULTS AND DISCUSSION

A. Magneto-optical imaging

Figure 1 summarizes the most representative results obtained by MOI for a FeSe crystal (upper row) and for a 9% S-doped FeSe crystal (lower row). Panels (a) and (e) show an optical microscopy image of the investigated samples. In (a) clear straight lines manifest the presence of terraces following the main crystallographic axes of the crystal. The second column in Fig. 1 [i.e., panels (b) and (f)] shows the magnetic field landscape obtained by the MOI technique at a magnetic field $H = 0.3$ mT, applied after cooling the sample down to 4 K. In these very weak fields, little flux penetration is observed into the sample, which is indicative of the Meissner phase. These images clearly illustrate that a macroscopic superconducting current is able to circulate in the entire sample surface and effectively screen the applied external field. This behavior contrasts with the field penetration in polycrystalline FeSe tapes, where a considerable distribution of T_c and weak-link features has been reported [31]. In the third column in Fig. 1, panels (c) and (g) show the magnetic field penetration at higher applied fields. Both samples exhibit a highly inhomogeneous field penetration. Indeed, the field advances into the sample by following two well-defined perpendicular directions. The fact that one of these directions is aligned with the observed terraces in the original optical image leads us to believe that the magnetic flux penetration is also aligned with the crystallographic axis of the orthorhombic structure. This is consistent with the recent finding of vortex trapping into twin planes in stoichiometric FeSe samples [32]. It is worth noting that the observed field penetration substantially departs from the critical state model typically applied for extracting the critical current density in hard type II superconductors. As such, critical currents obtained from macroscopic magnetization loops should be interpreted with caution [33]. In the rightmost column of Fig. 1 [panels (d) and (h)] the average intensity was recorded as a function of temperature in a square area of 50 μm $\times$ 50 μm in the center of the sample, which was set in a remanent state after field cooling in $H = 1$ mT and subsequently set $H = 0$ mT. From these measurements it is easy to identify the superconducting-to-normal transition. The onset of this transition agrees well with the values obtained by other global techniques such as specific heat, ac susceptibility, and resistivity.

B. Thermodynamic and transport properties

1. Effect of Co doping

Thermodynamic data of $FeSe_{1-x}S_x$ and $Fe_{1-x}Co_xSe$ are presented in Fig. 2. Figure 2(a) presents the magnetic susceptibility χ measured following zero-field-cooling (ZFC) and field-cooling procedures in an external field of 1 mT applied along the *c* axis. It is obvious that introducing small amounts of Co into the Fe site leads to suppression of the

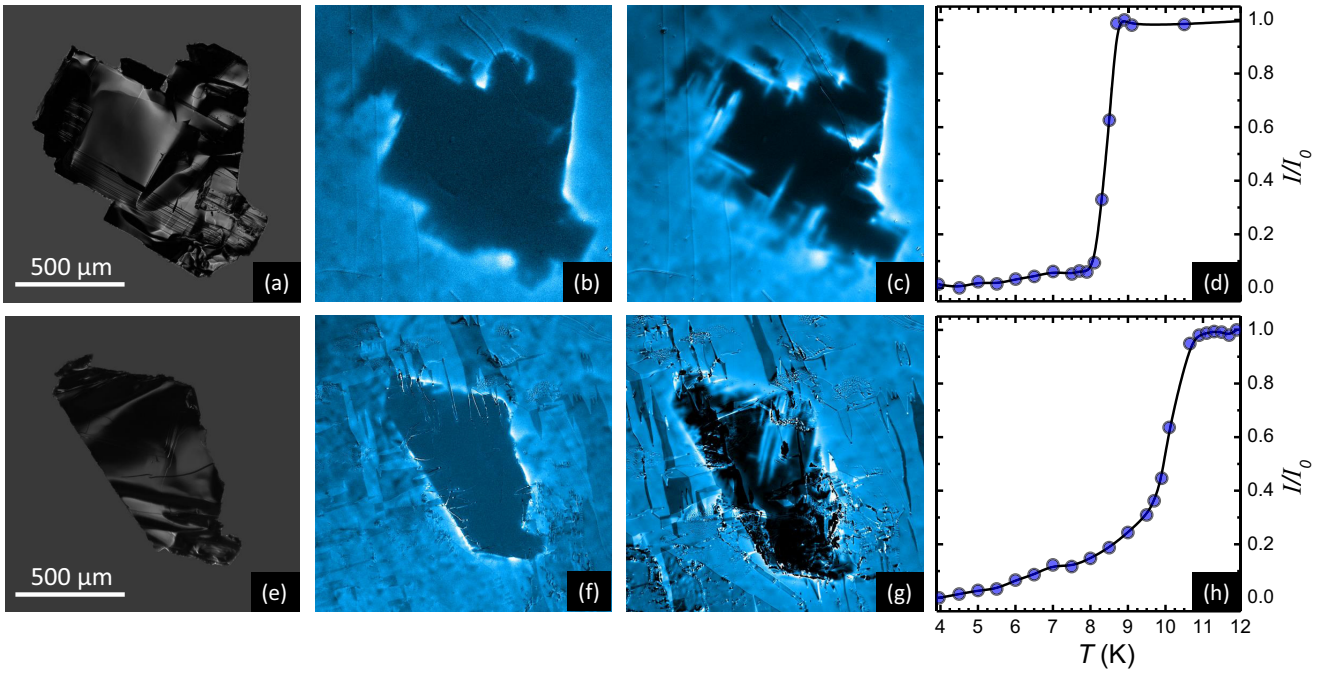

FIG. 1. MOI for FeSe (upper row) and $FeSe_{0.91}S_{0.09}$ (lower row). Panels (a) and (e) show optical images of the sample. Panels (b) and (f) show the magnetic flux distribution at 4 K for an applied field $H = 0.3$ mT, where bright (dark) areas correspond to high (low) magnetic fields. In panels (c) and (g), H is further increased and the flux penetration follows the crystallographic axes of the orthorhombic structure. T_c is determined in panels (d) and (h) by tracking the average intensity I as T is increased, in a 50×50 μm^2 square at the center of the sample. I is normalized by the intensity I_0 outside the sample.

superconducting transition temperature. This contrasts with the $FeSe_{1-x}S_x$ [8,27], where T_c first increases and then decreases as shown in Figs. 2(a) and 6. However, despite the suppression of superconductivity, no signatures of structural transitions are observed in the Co-doped samples with $x = 0.04$. In addition, this change of Se or Fe content not only leads to a different T_c [10], but also to slight changes from the ideal 1:1 ratio in FeSe, leading to severe changes of their superconducting properties. For instance, the low field magnetization data of various $FeSe_{1+\delta}$ samples showed that the strongest superconducting signal occurs for the most stoichiometric sample, whereas it has been shown that in the $FeSe_{0.82}$ case, there is no superconducting signal [34]. We should note that the suppression of the superconducting transition in Co-doped FeSe suggests the strong pair breaking effect of Co in heavily electron-doped FeSe. However, it is currently not certain whether Co in FeCoSe is a magnetic or nonmagnetic impurity. Although Co is generally considered as nonmagnetic in Fe-based superconductors, it is shown that Co may behave as magnetic impurities in overdoped $Ba(Fe,Co)_2As_2$ due to the incomplete charge transfer [35]. As shown from our results, the electron doping of 7% in Co-doped FeSe is limited by the solubility of Co. Some Co atoms that partially transfer electrons to FeSe may act as magnetic impurities. In addition, Co doping causes strong single particle scattering effects, which is also harmful to the superconductivity [36].

The temperature dependence of the specific heat as C_P/T vs T in zero field is shown in Fig. 2(b). The sharp diamagnetic signal in the ZFC data and the specific heat jump confirm bulk superconductivity in the investigated systems. In $Fe_{1-x}Co_xSe$, the estimated universal parameter $\Delta C_{el}/\gamma_n T_c$ of the specific heat at T_c is $\approx$2.14, 2.05, 2.12, and 1.82 mJ/mol K^2 for $x = 0$, 0.012, 0.024, and 0.04, respectively. These values are very close to the $FeSe_{1-x}S_x$ system [27]. The specific heat for $x = 0.07$ does not show any indication of superconductivity. This is very convenient because we can safely ignore the spin-fluctuation contribution to the specific heat in this system and can use it to remove the phonon contribution. However, jumps of specific heat at T_c in these materials are higher than the prediction of the weak-coupling Bardeen-Cooper-Schrieer (BCS) theory ($\Delta C_{\rm el}/\gamma_{\rm n} T_{\rm c} = 1.43$). As the superconducting transition is relatively sharp in our single crystals, a distribution in T_c or the presence of impurity phases cannot explain the large values of the normalized specific heat jump. Which may, instead, evidence the presence of a stronger-coupling strength in $Fe_{1-x}Co_xSe$. Additionally, as highlighted previously [27], the normalized specific heat jump reveals the presence of strong-coupling superconductivity in $FeSe_{1-x}S_x$. Figure 2(c) presents the temperature dependence of the ac susceptibilities for $Fe_{0.988}Co_{0.012}Se$. The measurements were done in an ac field with an amplitude $H_{ac} = 0.5$ mT and a frequency $f = 1$ kHz at different applied magnetic fields up to 9 T parallel to the c axis. The transition temperature T_c has been extracted from the bifurcation point between the real and imaginary parts of the ac susceptibilities χ' and χ''. In zero field, the superconducting transition is seen around 7.5 K, and shifts to lower T when the field is increased.

Figure 2(d) summarizes the temperature dependence of the upper critical field H_{c2} for the c orientation of the

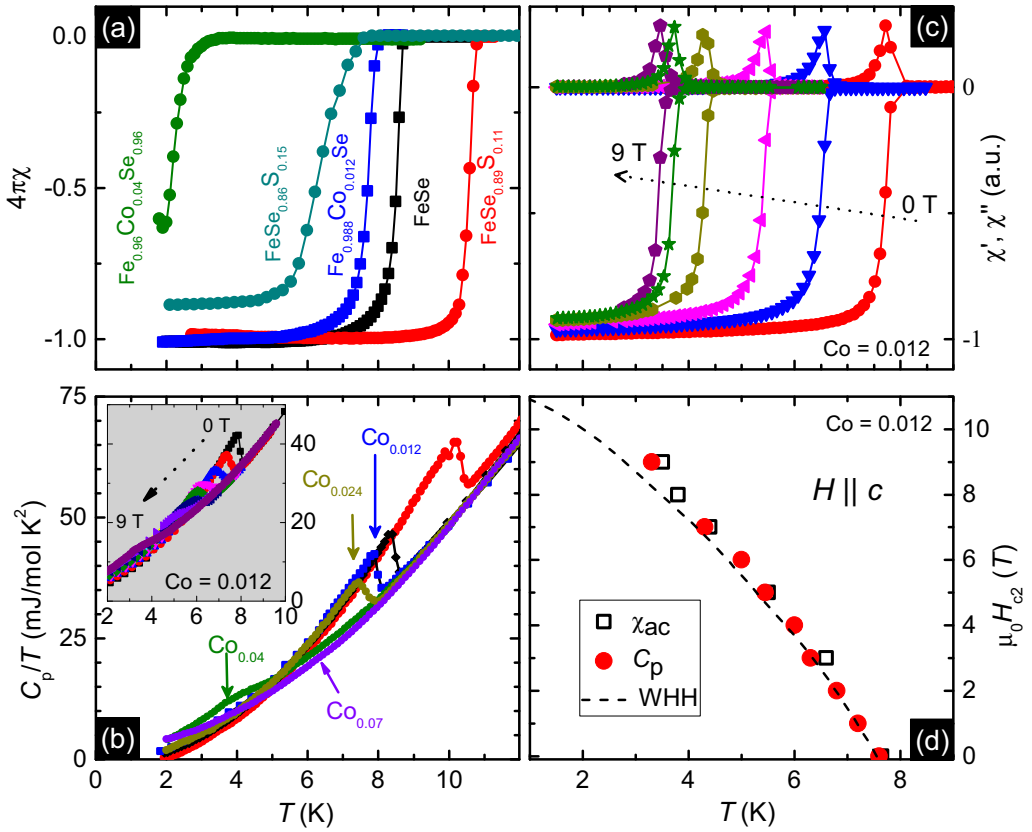

FIG. 2. (a) The temperature dependence of the magnetic susceptibility in an external field of 1 mT is applied along the c axis. The superconducting volume fraction (V_{fr}) is reduced by increased doping by either introducing Co or S to the FeSe system. (b) Temperature dependence of C_p/T vs T in zero magnetic field. The inset presents specific-heat data of $Fe_{0.98}Co_{0.012}Se$ in various applied magnetic fields up to 9 T parallel to the c axis. (c) The temperature dependence of the complex ac susceptibility components of $Fe_{0.98}Co_{0.012}Se$ measured in an ac field with an amplitude of 0.5 mT and a frequency of 1 kHz up to 9 T. The data was collected upon warming in different dc magnetic fields after cooling in a zero magnetic field. (d) Summarizes the phase diagram of H_{c2} vs temperature of $Fe_{0.98}Co_{0.012}Se$ for the field applied parallel to c. T_c has been estimated from an entropy-conserving construction and ac measurements. The open symbols are estimated from the ac magnetization, while the closed circles represent the specific heat. The dashed line represents the WHH model for $\lambda = 0$, $\alpha = 0$.

$Fe_{0.98}Co_{0.012}Se$ sample. The small differences observed between the data obtained from the specific heat and the ac magnetization for $H \parallel c$ are not surprising because these methods naturally imply different criteria for the T_c determination. In order to determine the upper critical field H_{c2} for the c orientation, we used the single-band Werthamer-Helfand-Hohenberg (WHH) formula [37] for an isotropic one-band BCS superconductor in the dirty limit. An example of WHH fitting is shown with the dashed line in Fig. 2(d). The WHH theory ($\alpha = 0$, $\lambda_{so} = 0$) predicts the behavior of $H_{c2}(T_c)$, where α is the Maki parameter which describes the relative strength of orbital breaking and the limit of paramagnetism, and λ_{so} is the spin-orbit scattering constant [37]. Using the data in Fig. 2(d), the upper critical field value at $T = 0$ for the $Fe_{0.98}Co_{0.012}Se$ system was evaluated to be $\approx$11.5 T. It is evident that the one-band WHH model fails to satisfy the extracted $H_{c2}(0)$. Using an additional two-band model with s-wave-like gaps, the temperature dependence of the electronic specific-heat data in $Fe_{1-x}Co_xSe$ can be well described, whereas single-gap BCS theory under the weak-coupling approach cannot describe our data (the data will be published elsewhere). Therefore, we believe that the observed deviation from the single-band WHH model is related to multiband effects in Co-doped FeSe.

2. *Structural transition*

To investigate the nature of tetragonal-to-orthorhombic phase transition in $FeSe_{1-x}S_x$, we conducted specific-heat and electrical resistivity ρ(T) measurements. Specific-heat data was collected up to 200 K for $FeSe_{1-x}S_x$ ($x = 0$, 0.04, and 0.11) and is presented in Fig. 3. Clear and sharp anomalies were resolved at the structural phase transition, hinting that an electronic structure transition took place, as a consequence of the nematic electronic transition. Data for the FeSe superconductors shows a very sharp orthorhombic phase transition at 87 K (upon heating), with a width of about 2 K. Upon S doping, the structural anomaly of the parent compound gradually shifted to lower temperatures down to 81 K and 72 K, for $x = 0.04$ and 0.11, respectively. The error in the determination of the T_s transition temperatures is estimated to be around 1 K when we consider the fact that the peak in the first derivative of the specific heat is relatively sharp. The specific heat anomaly at T_s gives $\Delta C_p/T_s \approx 5.57$, 5.43, and 4.1 mJ/mol K^2 for $x = 0.04$ and 0.11, respectively.

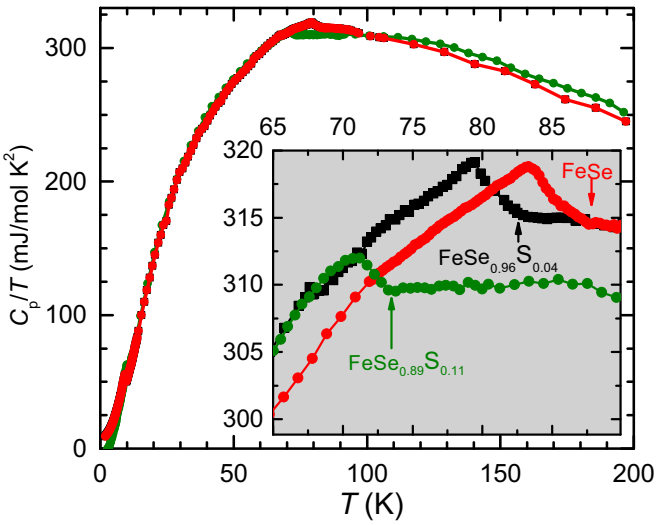

FIG. 3. Temperature dependence of specific heat with temperatures of up to 200 K for $FeSe_{1-x}S_x$ ($x = 0$, 0.04, and 0.11). The anomalies at higher temperatures which reflect the structural transition (see inset) are in agreement with the resistivity data.

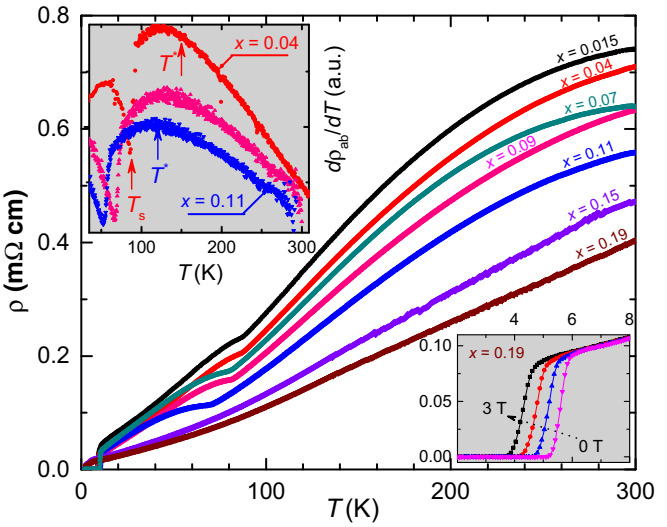

FIG. 4. In-plane resistivity of $FeSe_{1-x}S_x$ in a zero field. The upper inset presents the derivative of ρ for $x = 0.04$, 0.09, and 0.11. The arrows represent both T_s and the T^*. The lower inset shows the resistivity data for $FeS_{0.81}S_{0.19}$ in various applied magnetic fields up to 3 T, parallel to the c axis.

Interestingly, the value of these anomalies at T_s is very close to the Sommerfield coefficient, γ_n, at low temperature [27]. This can be directly linked to the reconstruction of the Fermi surface at T_s and reflects an electronic instability in our investigated systems. The electronic instability is supported by the field dependence of the magnetotransport at 12 K, which shows an abrupt sign change, suggesting a drastic reconstruction of the Fermi surfaces across the structural transition [38]. In addition, ARPES data at 30 K shows two holelike bands at the M point, in contrast with the single holelike band seen at 120 K [39]. This is likely caused by the formation of electronically driven nematic states.

The resistivity $\rho(T)$ for $FeSe_{1-x}S_x$ is shown in Fig. 4. All compounds are metals with resistivities ρ(250 K) varying from 0.708 mΩ cm for the parent compound (see Fig. 5) to 0.36, 0.52 mΩ cm for $x_S = 0.19$ and $x_{Co} = 0.04$, respectively. This reflects the good quality of the investigated crystals. The upper inset presents the derivative of resistivity curves for $x = 0.04$, 0.09, and 0.11. With increasing S doping, the nematicity is shifted to lower temperature and disappears under heavy doping. Simultaneously, the resistivity shows a drop at lower temperatures and zero resistivity at optimal doping with $T_c = 11.5$ K, indicating the coexistence of nematicity and superconductivity. This coexistence is observed up to $x = 0.15$ and no anomaly is associated with the nematic order for $x = 0.15$ and 0.19. The lower inset in Fig. 4 presents the temperature-dependence resistivity of $FeS_{0.81}S_{0.19}$ in various applied magnetic fields up to 3 T parallel to the c axis.

Another noteworthy peculiarity is the large variability of the room temperature resistivity of our investigated samples as shown in Fig. 4. It can be partially explained by the large error in the geometry factor but the ratio of resistivity of about 2.0 for samples with $x = 0$ and $x = 0.15$ definitely exceeds the possible error of our calculation. On the other hand, the absolute value of resistivity reported for pure FeSe differs significantly (more than three times over the value observed for $x = 0.19$). For example, the estimated room temperature value is changed from 0.4 m$\Omega \times$ cm to 1.7 m$\Omega \times$ cm [38]. However, the absolute value of resistivity was not precisely determined [38]. Therefore, it is not clear if the difference comes from systematic errors or from the resistivity dependence on any other (unknown) parameters, as for example, iron stoichiometry, impurity level, or chemical degradation in particular crystals. Nevertheless, based on our data there is a clear trend of a

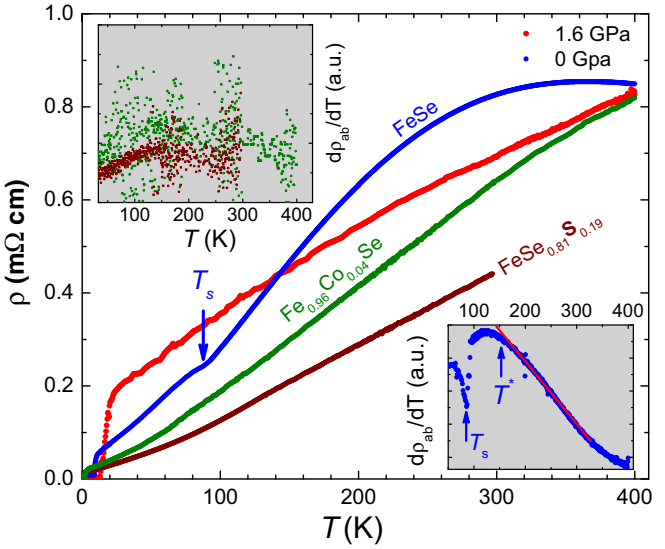

FIG. 5. The temperature dependence of the in-plane resistivity of FeSe by chemical and physical pressures in zero field. Increasing the pressure leads to a suppression of the nematic order state and to further suppression of the wide hump at higher temperature. The lower inset presents the derivative of an FeSe curve, displaying a sharp minima at T_s and maximum at T^*. The upper inset shows the derivative curves for $x_{Co} = 0.04$ and $x_S = 0.19$.

large resistivity decrease with sulfur substitution confirmed by presented curves and our other measurements. These results are very similar to those reported for the in-plane resistivity of FeSe single crystals under pressure [40]. With the application of pressure, the room temperature resistivity decreases by a factor of more than 3; it reaches a minimum at 10 GPa [40]. It is important to note that the residual resistance ratio in our cases, FeSeS, is not adequate due to the complex shape of $R(T)$. Nevertheless, in the case of the $x = 0.19$ sample, for which the $R(T)$ range is minimal, the ratio of resistivity at 10 K and 100 K is equal to 8, which is equivalent to about 25 at 300 K. However, the most important issue is the absence of any traces of impurity or defect scattering at low temperatures in measured $R(T)$ curves, which reflects the good quality of crystals.

3. *Chemical and physical pressure on FeSe*

In order to further explore the effect of pressure and doping on the FeSe single crystal, the temperature dependence of the in-plane resistivity of FeSe, $FeSe_{0.81}S_{0.19}$, and $Fe_{0.96}Co_{0.04}Se$ single crystals is summarized in Fig. 5. At the parent compound, resistivity decreases on cooling and shows an anomaly associated with the structural phase transition at $T_s \approx 86$ K and a sharp superconducting transition at $T_c \approx 8.9$ K. This is in agreement with the specific heat. It is obvious that the $d\rho/dT$ in FeSe at ambient pressure exhibits a remarkable feature with sharp minima at T_s and a maximum at T^* associated with a wide hump at high temperature, which shows a crossover from a probable semiconductinglike behavior to metallic behavior (see the inset in Fig. 5). A similar and consistent issue concerning the wide hump has been previously reported [6,41]. However, the origin of this crossover at high temperature could be associated with a change of carrier density. The values of T_s and T^* were obtained from the features in the resistivity derivative (insets of Figs. 3 and 4). However, the hump phenomenon has been found in other iron-selenide, $K_xFe_{2-y}Se_2$, superconductors [42,43], but it was not present in FeAs-based superconductors, where resistivity data for the pristine or doped compound exhibit a metallic behavior over the entire temperature range [44]. More interestingly, T_c, T_s, and the maximum in $d\rho/dT$ are suppressed by increasing the Co or S doping in FeSe. Upon compression to 1.6 GPa, the structural transition becomes significantly suppressed with increasing the pressure. Therefore, the structural transition in FeSe is initially suppressed under applied physical pressure with a similar manner to the chemical pressure effect of S substitution. A remarkable observation upon compression is the linear behavior of resistivity below 400 K, which is also reported for other Fe-based superconductors [45]. Nuclear magnetic resonance (NMR) measurements on FeSe show that with cooling below T_s spin fluctuations exist and even increase upon applying hydrostatic pressure [46]. Therefore, we cannot evidence the linear behavior of resistivity in FeSe upon compression with the strength of antiferromagnetic spin fluctuations.

C. Electronic phase diagram

Using the experimental results of the thermodynamic and electrical resistivity data, we summarize the evolution of the distinct features of impurity scattering in the FeSe system. The T_c, T_s, and T^* of $FeSe_{1-x}S_x$ single crystals, as a function of the S content, are shown in Fig. 6. Both T_s and the maximum of the $d\rho(T)/dT$, T^*, are intimately linked, even for under/optimal doping. In the overdoped regime these linked features are suppressed by doping and disappear at $x = 0.15$. However, we shallow the area of the T^* in the main panel of Fig. 6. The inset of Fig. 6 illustrates the electronic phase diagram of $Fe_{1-x}Co_xSe$. This correlated suppression of both T_s and T_c could be related to the orbital fluctuation induced by either Co or S substitutions. Additionally, the nesting between electron and hole pockets plays an important role in this suppression of structural ordering in Fe-based superconductors [18,47]. In our case upon S doping and once nematicity is suppressed, superconductivity starts to decrease. Concentrations shows suppression of both nematicity and superconductivity in FeSe. This is in contrast to Co-doped $Ba(Fe_{1-x}Co_x)_2As_2$ where superconductivity is enhanced instead by the suppression [22]. Therefore, we think that we cannot rule out other roles of charge doping besides suppressing nematicity. Although the K-dosed FeSe and FeSe under high pressure both show suppressed nematicity and an enhanced T_c around 40 K, they are different in several important regards: (i) The K-dosed FeSe is heavily electron doped with only electron Fermi surfaces, while the FeSe under pressure should be undoped with very different Fermi-surface topology, and (ii) FeSe under high pressure shows a compressed lattice and reduced anion height, due to the external pressure, compared with K-dosed FeSe.

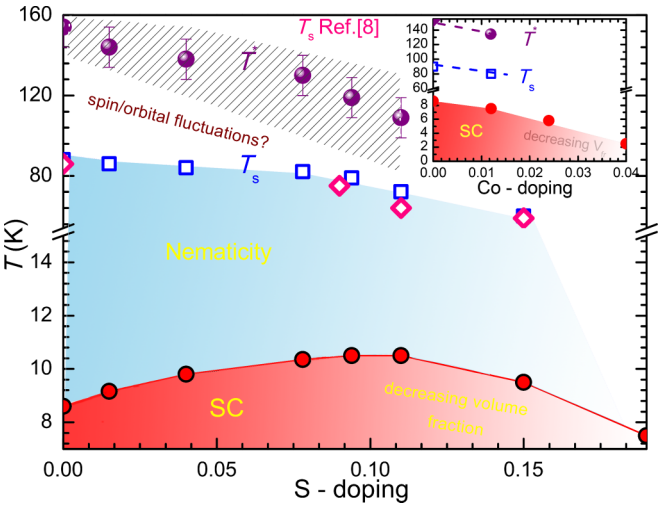

FIG. 6. The S concentration (x) dependence of the superconducting transition temperature (T_c), structural transition (T_s), and the T^* obtained from magnetic, specific-heat, and electric resistivity data. T_s is compared to values reported in Ref [8]. The phase diagram highlights the suppression of T_s and the transition at T^* by increasing the S concentration. The inset summarizes the Co concentration dependence, in which the T_c decreases upon increasing doping.

Despite this, whether the nematic order is driven by a spin or an orbital fluctuation remains controversial. If orbital ordering is the efficient cause, the phase below the nematic breaks C_4 symmetry, and quantum fluctuations associated with this phase are nematic in character [48–50]. However, the resistivity data exhibits a non-Fermi-liquid-like behavior above T_c, which would suggest orbital fluctuations exist below the nematic

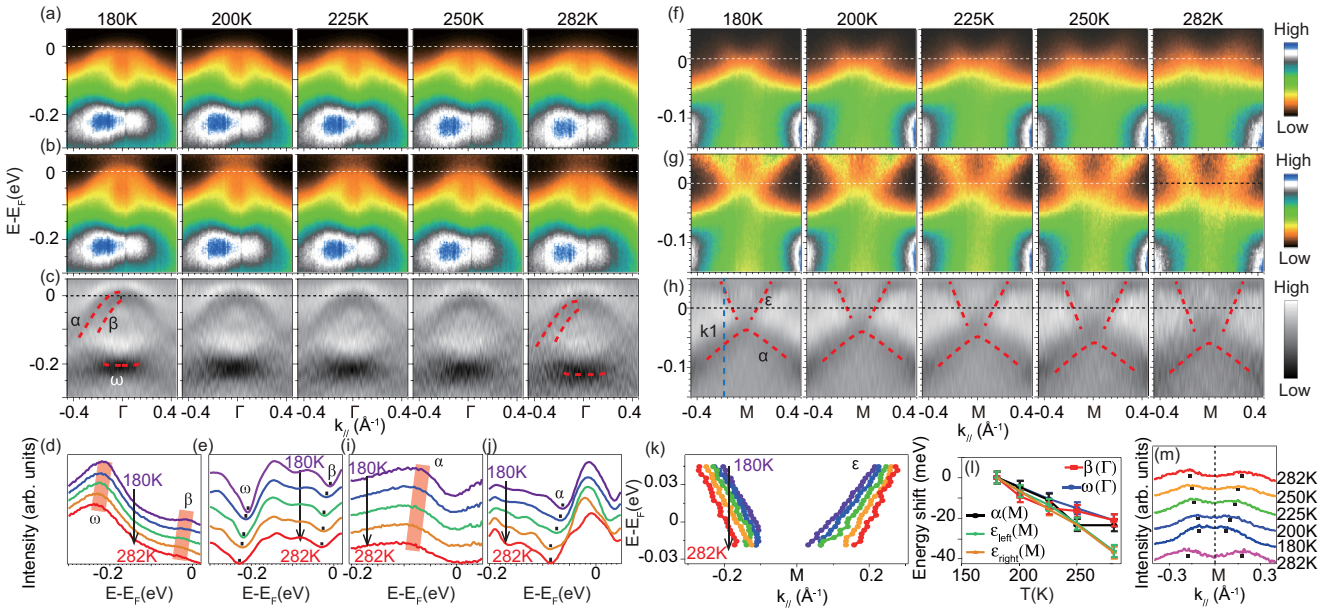

FIG. 7. The temperature dependence of the band structure of $FeSe_{1-x}S_x$ ($x = 0.055$): (a) Temperature dependence of the photoemission spectra around Γ, (b) the spectra divided by the energy-resolution-convoluted Fermi-Dirac function, and (c) their second derivative with respect to energy. The red dashed lines are local minimum locus to indicate the band position of α, β, and ω. (d) The energy distribution curves (EDCs) divided by the energy-resolution-convoluted Fermi-Dirac function at Γ with varied temperature. (e) The second derivative of the EDCs in panel (d), the positions of the band top of β, and ω are obtained by tracking the local minimum locus of the EDCs. (f)–(h) are the same as (a)–(c), respectively, but around M, the red dashed curves indicate the dispersion of α, ϵ. (i) The same as panel (d), but at k1. The momentum position of k1 is indicated in panel (h). (j) The same as (e), but at k1. The energy positions of α at k1 is obtained by tracking the local minimum locus of the EDCs. (k) The temperature dependence of the dispersion of the ϵ band, which is obtained by tracking the local maximum locus of the momentum distribution curves (MDCs) at different temperatures. (l) The energy shifts as a function of temperature for the different bands. (m) The MDCs integrated near Fermi energy (E_F) over ($E_F - 10$ meV, $E_F + 10$ meV) with a loop in temperature.

order [49]. Additionally, there is no change of the T_s anomaly under 9 T in transport and specific-heat measurements of FeSe (not shown), which might indicate that spin fluctuations are not involved directly in the structural transition. However, recent sound experimental studies on the origin of the nematic phase in iron chalcogenides reach opposing conclusions and this question remains highly debated. Experimental evidence of the existence of strong nematic fluctuations up to 200 K has been reported in $Ba(Fe,Co)_2As_2$ [51]. However, NMR measurements suggest the absence of spin fluctuations above T_s in the tetragonal phase and spontaneous orbital order has been invoked which explains the nematic state in FeSe [7,9]. In contrast to the NMR data, recent neutron scattering measurements reveal substantial spin fluctuations in the tetragonal phase in FeSe [52]. These measurements demonstrate that the absence of spin fluctuations suggested by NMR is simply due to the opening of a 2.5 meV spin gap in a quantum nematic paramagnetic state (NMR only probes very low energy spin fluctuations). Furthermore, very recently, Glasbrenner *et al.* [53] have shown that the long-range magnetic ordering in FeSe is prevented by the excitation of spin fluctuations, but allows the usual spin-driven nematic order. Additionally, the spin-driven nematic order is also accompanied by a ferro-orbital order.

D. ARPES

A noticeable change in the electronic properties of FeSeS is observed in our transport and thermodynamic data. This can be consistently explained by the Fermi-surface reconstruction under sulfur substitution. The Lifshitz-type quantum transition can be a possible source of changes in absolute values of resistivity and suppression of certain power terms in the low temperature $R(T)$ expansion. According to our data the transition can happen between 5% and 10% of sulfur substitution. Therefore, to check this possibility the microscopic properties of Fe(SeS) should be addressed. However, to comprehend the T^* in the main panel of Fig. 6, it is also very interesting to comprehend the real band structure. Additionally, the hump at elevated temperatures seems to be a standard feature of any degenerated semiconductors observed many times in various systems [54], which only reflects the crossover between semiconducting and metallic behavior. In order to further explore this behavior at higher temperature above structural transition, we performed ARPES measurements at different temperatures above the nematic transition temperature in $FeSe_{1-x}S_x$ single crystals for $x = 0.055$. From the temperature dependence of band structure around Γ shown in Figs. 7(a)–7(c), the generic features for all the different temperatures include two parabolic bands noted as α and β near E_F, and a relative flat band noted as ω at high binding energy. An energy shift of bands exists with increasing temperature [Figs. 7(a)–7(c)]. At 180 K, the top of the hole band α around Γ is slightly above E_F within 10 meV and the top of the hole band β around Γ is about 7 meV below E_F [Fig. 7(c)]. At 282 K, both α and β completely sink below the E_F [Fig. 7(c)], indicating a temperature-induced Lifshitz transition, similar to those in $Ba(Fe,Co)_2As_2$ [55] and

in WTe_2 [56]. Note that the band tops of α and β are within the energy scale of the thermal excitation; these bands still contain hole carriers at 282 K although they have shifted below E_F [55]. Quantitatively, as shown in Figs. 7(d) and 7(e), the energy shifts of the β band and the ω band at Γ are remarkably similar. It should be noted that the temperature of the Lifshitz transition is much higher than the temperature for the nematic transition.

As shown in the temperature dependence of band structures around M [Figs. 7(f)–7(h)], the generic features for all the different temperatures include an electronlike band noted as ϵ near E_F, and a parabolic band noted as α at high binding energy. At 180 K, the bottom of ϵ is $\approx$35 meV below E_F [Fig. 7(h)]. In Figs. 7(f)–7(h), an energy shift of the two bands exists with increasing temperature. As shown by the energy distribution curves (EDCs) at k1 in Figs. 7(i)–7(j), α gradually shifts to higher binding energies with increasing temperature. Moreover, band ϵ shifts to higher binding energies rigidly [Fig. 7(k)]. As shown by the quantitative analysis of energy shifts in Fig. 7(l), all bands near Γ and M shift similarly with increasing temperature, indicating a temperature-induced chemical potential shift, i.e., a Lifshitz transition, involving a change of the Fermi-surface topology in FeSeS. The temperature cycle measurement between 282 K and 180 K [Fig. 7(m)] demonstrates that the temperature-induced chemical potential shift is intrinsic.

The temperature-induced chemical potential shift has been observed in several materials, such as $Ba(Fe,Co)_2As_2$ [55], $Ba(Fe,Ru)_2As_2$ [57], and WTe_2 [56,58]. The origin of the shift has been explained by the thermal excitations of carriers in semimetals, where the top of the hole bands and bottom of the electron bands are close to the chemical potential within the energy range of thermal broadening. As calculations show in [55,56], the numbers of hole and electron carriers both increase with increasing temperature due to thermal excitation. However, if the chemical potential μ were fixed, the increased number would have been different for hole and electron carriers according to the calculations [55,56]. To avoid this, charge carriers redistribute from holes to electrons to keep the conservation of the net charge of carriers (proportional to the filling), resulting in the chemical potential shift and a Lifshitz transition [55,56]. For FeSeS, the observed semimetal behavior of the electronic structure meets the prerequisite of the scenario proposed in Refs. [55,56], and can qualitatively explain the shift of chemical potential observed here.

IV. CONCLUSION

To summarize, from extensive thermodynamics, transport, and ARPES studies, we report on the effect of Co and S substitution on the superconductivity and structural transition/orbital order in FeSe. Furthermore, images of the magnetic flux penetration in the whole sample show that it strongly departs from the Bean critical state model, often applied to hard type-II superconductors such as iron-based superconductors. We demonstrate that $\Delta C_p/T_s \approx \gamma_n$ in S-doped systems due to the reconstruction of the Fermi surface at T_s, which reflects an electronic instability in this system. We have shown that FeSe exhibits remarkable features with a wide hump at high temperature, suppressed by Co or S doping or external pressure. This hump, together with the nematic order, was suppressed by further doping. Our ARPES data between 180 K and 282 K indicate that chemical potential shift with increasing thermal excitations exists, resulting in a change of the Fermi-surface topology. In addition, the temperature-induced Lifshitz transition is similar to WTe_2 and $Ba(Fe,Co)_2As_2$ is observed. Our results establish the correlation between superconductivity and the nematicity.

ACKNOWLEDGMENTS

We are grateful to Alexander Kordyuk and Goran Karapetrov for stimulating discussions. The work in Germany was supported by program MO 3014/1-1 of the DFG. The work in Russia was supported in part by the Ministry of Education and Science of the Russian Federation in the framework of Increase Competitiveness Program of NUST "MISiS" (K2-2015-075), and by Act 211 of the Russian Federation Government, Contract No. 02.A03.21.0006. J.B. acknowledges support from F.R.S.-FNRS (Research Fellowship). The work of A.V.S. has been partially supported by the "Mandat d'Impulsion Scientifique" MIS F.4527.13 from F.R.S.-FNRS.

[1] R. M. Fernandes, A. V. Chubukov, and J. Schmalian, What drives nematic order in iron-based superconductors?, Nat. Phys. **10**, 97 (2014).

[2] P. C. Dai, J. P. Hu, and E. Dagotto, Magnetism and its microscopic origin in iron-based high-temperature superconductors, Nat. Phys. **8**, 709 (2012).

[3] D. Parker, M. G. Vavilov, A. V. Chubukov, and I. I. Mazin, Coexistence of superconductivity and a spin-density wave in pnictide superconductors: Gap symmetry and nodal lines, Phys. Rev. B **80**, 100508(R) (2009).

[4] M. Bendele, A. Ichsanow, Yu. Pashkevich, L. Keller, Th. Strassle, A. Gusev, E. Pomjakushina, K. Conder, R. Khasanov, and H. Keller, Coexistence of superconductivity and magnetism in $FeSe_{1-x}$ under pressure, Phys. Rev. B **85**, 064517 (2012).

[5] M. Bendele, A. Amato, K. Conder, M. Elender, H. Keller, H.-H. Klauss, H. Luetkens, E. Pomjakushina, A. Raselli, and R. Khasanov, Pressure Induced Static Magnetic Order in Superconducting $FeSe_{1-x}$, Phys. Rev. Lett. **104**, 087003 (2010).

[6] F.-C. Hsu, J.-Y. Luo, K.-W. Yeh, T.-K. Chen, T.-W. Huang, P. M. Wu, Y.-C. Lee, Y.-L. Huang, Y.-Y. Chu, D.-C. Yan, and M.-K. Wu, Superconductivity in the PbO-type structure α-FeS, Proc. Natl. Acad. Sci. U.S.A. **105**, 14262 (2008).

[7] S.-H. Baek, D. V. Efremov, J. M. Ok, J. S. Kim, J. van den Brink, and B. Büchner, Orbital-driven nematicity in FeSe, Nat. Mater. **14**, 210 (2015).

[8] M. D. Watson, T. K. Kim, A. A. Haghighirad, S. F. Blake, N. R. Davies, M. Hoesch, T. Wolf, and A. I. Coldea, Suppression of orbital ordering by chemical pressure in $FeSe_{1-x}S_x$, Phys. Rev. B **92**, 121108(R) (2015).

[9] A. E. Böhmer, T. Arai, F. Hardy, T. Hattori, T. Iye, T. Wolf, H. v. Löhneysen, K. Ishida, and C. Meingast, Origin of the Tetragonal-to-Orthorhombic Phase Transition in FeSe: A Combined Thermodynamic and NMR Study of Nematicity, Phys. Rev. Lett. **114**, 027001 (2015).

[10] T. M. McQueen, A. J. Williams, P. W. Stephens, J. Tao, Y. Zhu, V. Ksenofontov, F. Casper, C. Felser, and R. J. Cava, Tetragonal-to-Orthorhombic Structural Phase Transition at 90 K in the Superconductor $Fe_{1.01}Se$, Phys. Rev. Lett. **103**, 057002 (2009).

[11] S. Y. Tan *et al.*, Interface-induced superconductivity and strain-dependent spin density waves in FeSe/$SrTiO_3$ thin films, Nat. Mater. **12**, 634 (2013).

[12] R. Peng, X. P. Shen, X. Xie, H. C. Xu, S. Y. Tan, M. Xia, T. Zhang, H. Y. Cao, X. G. Gong, J. P. Hu, B. P. Xie, and D. L. Feng, Measurement of an Enhanced Superconducting Phase and a Pronounced Anisotropy of the Energy Gap of a Strained FeSe Single Layer in FeSe/Nb: $SrTiO_3$/$KTaO_3$ Heterostructures using Photoemission Spectroscopy, Phys. Rev. Lett. **112**, 107001 (2014).

[13] J. J. Lee, F. T. Schmitt, R. G. Moore, S. Johnston, Y.-T. Cui, W. Li, M. Yi, Z. K. Liu, M. Hashimoto, Y. Zhang, D. H. Lu, T. P. Devereaux, D.-H. Lee, and Z.-X. Shen, Interfacial mode coupling as the origin of the enhancement of T_c in FeSe films on $SrTiO_3$, Nature (London) **515**, 245 (2014).

[14] C. H. P. Wen, H. C. Xu, C. Chen, Z. C. Huang, Y. J. Pu, Q. Song, B. P. Xie, Mahmoud Abdel-Hafiez, D. A. Chareev, A. N. Vasiliev, R. Peng, and D. L. Feng, Anomalous correlation effects and unique phase diagram of electron doped FeSe revealed by angle resolved photoemission spectroscopy, Nat. Commun. **7**, 10840 (2016).

[15] V. Mishra, Effect of disorder on superconductivity in the presence of spin-density wave order, Phys. Rev. B **91**, 104501 (2015).

[16] S. Onari and H. Kontani, Violation of Anderson's Theorem for the Sign-Reversing s-Wave State of Iron-Pnictide Superconductors, Phys. Rev. Lett. **103**, 177001 (2009).

[17] Q. Zhang *et al.*, Neutron-Scattering Measurements of the Spin Excitations in LaFeAsO and $Ba(Fe_{0.953}Co_{0.047})_2As_2$: Evidence for a Sharp Enhancement of Spin Fluctuations by Nematic Order, Phys. Rev. Lett. **114**, 057001 (2015).

[18] H. Kontani and S. Onari, Orbital-Fluctuation-Mediated Superconductivity in Iron Pnictides: Analysis of the Five-Orbital Hubbard-Holstein Model, Phys. Rev. Lett. **104**, 157001 (2010).

[19] W. Rowe, I. Eremin, A. T. Rømer, B. M. Andersen, and P. J. Hirschfeld, Doping asymmetry of superconductivity coexisting with antiferromagnetism in spin fluctuation theory, New J. Phys. **17**, 023022 (2015).

[20] J. Schmiedt, P. M. R. Brydon, and C. Timm, Superconducting pairing in the spin-density-wave phase of iron pnictides, Phys. Rev. B **89**, 054515 (2014).

[21] T. Urata, Y. Tanabe, K. K. Huynh, Y. Yamakawa, H. Kontani, and K. Tanigaki, Argument on superconductivity pairing mechanism from cobalt impurity doping in FeSe: Spin (s) or orbital (s_{++}) fluctuation, Phys. Rev. B **93**, 014507 (2016).

[22] F. Kurth, K. Iida, S. Trommler, J. Hnisch, K. Nenkov, J. Engelmann, S. Oswald, J. Werner, L. Schultz, and B. Holzapfel, Electronic phase diagram of disordered Co doped $BaFe_2As_{2-d}$, Supercond. Sci. Technol. **26**, 025014 (2013).

[23] Q. A. Li, K. E. Gray, H. Zheng, H. Claus, S. Rosenkranz, S. Nyborg Ancona, R. Osborn, J. F. Mitchell, Y. Chen, and J. W. Lynn, Reentrant Orbital Order and the True Ground State of $LaSr_2Mn_2$, Phys. Rev. Lett. **98**, 167201 (2007).

[24] R. Busch, G. Ries, H. Werthner, G. Kreiselmeyer, and G. Saemann-Ischenko, New Aspects of the Mixed State from Six-Terminal Measurements on $Bi_2Sr_2CaCu_2O_x$ Single Crystals, Phys. Rev. Lett. **69**, 522 (1992).

[25] D. Chareev, E. Osadchii, T. Kuzmichev, J.-Y. Lin, S. Kuzmichev, O. Volkova, and A. Vasiliev, Single crystal growth and characterization of tetragonal $FeSe_{1-x}$ superconductors, CrystEngComm **15**, 1989 (2013).

[26] J.-Y. Lin, Y. S. Hsieh, D. A. Chareev, A. N. Vasiliev, Y. Parsons, and H. D. Yang, Coexistence of isotropic and extended s-wave order parameters in FeSe as revealed by low-temperature specific heat, Phys. Rev. B **84**, 220507(R) (2011).

[27] M. Abdel-Hafiez, Y.-Y. Zhang, Z.-Y. Cao, C.-G. Duan, G. Karapetrov, V. M. Pudalov, V. A. Vlasenko, A. V. Sadakov, D. A. Knyazev, T. A. Romanova, D. A. Chareev, O. S. Volkova, A. N. Vasiliev, and X.-J. Chen, Superconducting properties of sulfur-doped iron selenide, Phys. Rev. B **91**, 165109 (2015).

[28] M. Abdel-Hafiez, J. Ge, A. N. Vasiliev, D. A. Chareev, J. Van de Vondel, V. V. Moshchalkov, and A. V. Silhanek, Temperature dependence of lower critical field $H_{c1}(T)$ shows nodeless superconductivity in FeSe, Phys. Rev. B **88**, 174512 (2013).

[29] C. Jooss, J. Albrecht, H. Kuhn, S. Leonhardt, and H. Kronmüller, Magneto-optical studies of current distributions in high-T_c superconductors, Rep. Prog. Phys. **65**, 651 (2002).

[30] M. R. Koblischka and R. J. Wijngaarden, Magneto-optical investigations of superconductors, Supercond. Sci. Technol. **8**, 199 (1995).

[31] Q.-P. Ding, S. Mohan, Y. Tsuchiya, T. Taen, Y. Nakajima, and T. Tamegai, Magneto-optical imaging and transport properties of FeSe superconducting tapes prepared by diffusion method, Supercond. Sci. Technol. **25**, 025003 (2012).

[32] Can-Li Song, Yi-Lin Wang, Ye-Ping Jiang, Lili Wang, Ke He, Xi Chen, Jennifer E. Hoffman, Xu-Cun Ma, and Qi-Kun Xue, Suppression of Superconductivity by Twin Boundaries in FeSe, Phys. Rev. Lett. **109**, 137004 (2012); T. Watashige *et al.*, Evidence for Time-Reversal Symmetry Breaking of the Superconducting State near Twin-Boundary Interfaces in FeSe Revealed by Scanning Tunneling Spectroscopy, Phys. Rev. X **5**, 031022 (2015).

[33] Y. Sun, S. Pyon, T. Tamegai, R. Kobayashi, T. Watashige, S. Kasahara, Y. Matsuda, and T. Shibauchi, Critical current density, vortex dynamics, and phase diagram of FeSe single crystal, Phys. Rev. B **92**, 144509 (2015).

[34] A. J. Williams, T. M. McQueen, and R. J. Cava, The stoichiometry of FeSe, Solid State Commun. **149**, 1507 (2009).

[35] M. L. Teague, G. K. Drayna, G. P. Lockhart, P. Cheng, B. Shen, H.-H. Wen, and N.-C. Yeh, Measurement of a Sign-Changing Two-Gap Superconducting Phase in Electron-Doped $Ba(Fe,Co)_2As_2$ Single Crystals Using Scanning Tunneling Spectroscopy, Phys. Rev. Lett. **106**, 087004 (2011).

[36] Z. R. Ye, Y. Zhang, F. Chen, M. Xu, J. Jiang, X. H. Niu, C. H. P. Wen, L. Y. Xing, X. C. Wang, C. Q. Jin, B. P. Xie, and D. L. Feng, Extraordinary Doping Effects on Quasiparticle Scattering and Bandwidth in Iron-Based Superconductors, Phys. Rev. X **4**, 031041 (2014).

[37] N. R. Werthamer, E. Helfand, and P. C. Hohenberg, Temperature and purity dependence of the superconducting critical field, H_{c2}. III. Electron spin and spin-orbit effects, Phys. Rev. **147**, 295 (1966).

[38] K. K. Huynh, Y. Tanabe, T. Urata, H. Oguro, S. Heguri, K. Watanabe, and K. Tanigaki, Electric transport of a single-crystal iron chalcogenide FeSe superconductor: Evidence of symmetry-breakdown nematicity and additional ultrafast Dirac cone-like carriers, Phys. Rev. B **90**, 144516 (2014).

[39] K. Nakayama, Y. Miyata, G. N. Phan, T. Sato, Y. Tanabe, T. Urata, K. Tanigaki, and T. Takahashi, Reconstruction of Band Structure Induced by Electronic Nematicity in an FeSe Superconductor, Phys. Rev. Lett. **113**, 237001 (2014).

[40] H. Okabe, N. Takeshita, K. Horigane, T. Muranaka, and J. Akimitsu, Pressure-induced high-T_c superconducting phase in FeSe: Correlation between anion height and T_c, Phys. Rev. B **81**, 205119 (2010).

[41] Y. Imai, Y. Sawada, F. Nabeshima, and A. Maeda, Suppression of phase separation and giant enhancement of superconducting transition temperature in $FeSe_{1-x}Te_x$ thin films, Proc. Natl. Acad. Sci. U.S.A. **112**, 1937 (2015).

[42] J. Guo *et al.*, Pressure-Driven Quantum Criticality in Iron-Selenide Superconductors, Phys. Rev. Lett. **108**, 197001 (2012).

[43] D. M. Wang, J. B. He, T.-L. Xia, and G. F. Chen, Effect of varying iron content on the transport properties of the potassium-intercalated iron selenide $K_xFe_{2-y}Se_2$, Phys. Rev. B **83**, 132502 (2011).

[44] L. Harnagea *et al.*, Phase diagram of the iron arsenide superconductors $Ca(Fe_{1-x}Co_x)_2As_2 (0 \leqslant x \leqslant 0.2)$, Phys. Rev. B **83**, 094523 (2011).

[45] S. Kasahara, T. Shibauchi, K. Hashimoto, K. Ikada, S. Tonegawa, R. Okazaki, H. Shishido, H. Ikeda, H. Takeya, K. Hirata, T. Terashima, and Y. Matsuda, Evolution from non-Fermi- to Fermi-liquid transport via isovalent doping in $BaFe_2(As_{1-x}P_x)_2$ superconductors, Phys. Rev. B **81**, 184519 (2010).

[46] T. Imai, K. Ahilan, F. L. Ning, T. M. McQueen, and R. J. Cava, Why Does Undoped FeSe Become a High-T_c Superconductor under Pressure?, Phys. Rev. Lett. **102**, 177005 (2009).

[47] K. Kuroki, S. Onari, R. Arita, H. Usui, Y. Tanaka, H. Kontani, and H. Aoki, Unconventional Pairing Originating from the Disconnected Fermi Surfaces of Superconducting $LaFeAsO_{1-x}F_x$, Phys. Rev. Lett. **101**, 087004 (2008).

[48] F. Kruger, S. Kumar, J. Zaanen, and J. van den Brink, Spin-orbital frustrations and anomalous metallic state in iron-pnictide superconductors, Phys. Rev. B **79**, 054504 (2009).

[49] W.-C. Lee and P. W. Phillips, Non-Fermi liquid due to orbital fluctuations in iron pnictide superconductors, Phys. Rev. B **86**, 245113 (2012).

[50] C.-C. Lee, W.-G. Yin, and W. Ku, Ferro-Orbital Order and Strong Magnetic Anisotropy in the Parent Compounds of Iron-Pnictide Superconductors, Phys. Rev. Lett. **103**, 267001 (2009).

[51] L. Stojchevska, T. Mertelj, J.-H. Chu, I. R. Fisher, and D. Mihailovic, Doping dependence of femtosecond quasiparticle relaxation dynamics in $Ba(Fe,Co)_2As_2$ single crystals: Evidence for normal-state nematic fluctuations, Phys. Rev. B **86**, 024519 (2012).

[52] Q. Wang, Y. Shen, B. Pan, Y. Hao, M. Ma, F. Zhou, P. Steffens, K. Schmalzl, T. R. Forrest, M. Abdel-Hafiez, X. J. Chen, D. A. Chareev, A. N. Vasiliev, P. Bourges, Y. Sidis, H. Cao, and J. Zhao, Strong interplay between stripe spin fluctuations, nematicity and superconductivity in FeSe, Nat. Mater. **15**, 159 (2016).

[53] J. K. Glasbrenner, I. I. Mazin, H. O. Jeschke, P. J. Hirschfeld, R. M. Fernandes, and R. Valenti, Effect of magnetic frustration on nematicity and superconductivity in iron chalcogenides, Nat. Phys. **11**, 953 (2015).

[54] N. B. Brandt and V. A. Kulbachinskii, Pressure spectroscopy of impurity states and band structure of bismuth telluride, Semicond. Sci. Technol. **7**, 907 (1992).

[55] V. Brouet, Ping-Hui Lin, Y. Texier, J. Bobroff, and A. Taleb-Ibrahimi, Large Temperature Dependence of the Number of Carriers in Co-Doped $BaFe_2As_2$, Phys. Rev. Lett. **110**, 167002 (2013).

[56] Yun Wu, Na Hyun Jo, M. Ochi, L. Huang, and D. Mou, Temperature-Induced Lifshitz Transition in WTe_2, Phys. Rev. Lett. **115**, 166602 (2015).

[57] R. S. Dhaka, S. E. Hahn, E. Razzoli, Rui Jiang, M. Shi, B. N. Harmon, A. Thaler, S. L. Bud'ko, P. C. Canfield, and A. Kaminski, Unusual Temperature Dependence of Band Dispersion in $Ba(Fe_{1-x}Ru_x)_2As_2$ and its Consequences for Antiferromagnetic Ordering, Phys. Rev. Lett. **110**, 067002 (2013).

[58] I. Pletikosic, Mazhar N. Ali, A. V. Fedorov, R. J. Cava, and T. Valla, Electronic Structure Basis for the Extraordinary Magnetoresistance in WTe_2, Phys. Rev. Lett. **113**, 216601 (2014).